THE JOURNAL OF PHYSICAL CHEMISTRY C
A JOURNAL OF THE AMERICAN CHEMICAL SOCIETY

pubs.acs.org/JPCC

Article

Factors Influencing Preferential Anion Interactions during Solvation of Multivalent Cations in Ethereal Solvents

Published as part of The Journal of Physical Chemistry virtual special issue "Hellmut Eckert Festschrift".

Kee Sung Han,[#] Nathan T. Hahn,[#] Kevin R. Zavadil, Nicholas R. Jaegers, Ying Chen, Jian Zhi Hu, Vijayakumar Murugesan,* and Karl T. Mueller*

Cite This: *J. Phys. Chem. C* 2021, 125, 6005−6012

Read Online

ACCESS | Metrics & More | Article Recommendations | Supporting Information

ABSTRACT: Most multivalent secondary batteries have employed electrolytes composed of cyclic ether solvents such as tetrahydrofuran or linear glycol ether solvents (glymes) such as 1,2-dimethoxyethane (G1). A robust understanding of multivalent cation solvation tendencies in these classes of solvents provides insight into corresponding structure−property relationships which, in turn, promotes the design and discovery of improved electrolytes. In this work, our goal is to systematically address how electrolyte constituent properties, namely, ether solvent structure and dication size, direct the solvation interactions of divalent electrolytes and their resultant properties. This study utilizes pulsed-field gradient (PFG) nuclear magnetic resonance (NMR) spectroscopy in conjunction with Raman spectroscopy and ionic conductivity measurements to elucidate the preferential interactions between multivalent cations, anions, and solvent molecules along with their correlated ion dynamics. These investigations incorporate two representative divalent cations (Ca^{2+} and Zn^{2+}) as well as two ethereal solvent representatives from both the cyclic ether and glyme structural classes. The results reveal that anions coordinate more readily with divalent cations in cyclic ethers than in glymes. Furthermore, the coordination of the anions with Ca^{2+}, i.e., contact-ion pair (CIP) formation is more pronounced than with Zn^{2+} in a glyme solvent of limited chain length (G1), providing insight into cation size effects that are important for translating solvation behavior across various multivalent electrolytes. Importantly, we find that specific anion coordination is more strongly controlled by solvent structure than by salt concentration in the practical range of 0.1−0.5 M. However, simply reducing these inner-sphere inter-ionic interactions by changing solvent structure does not necessarily de-correlate ionic motion. Instead, concentration-dependent changes in molar ionic conductivity suggest that second-shell interactions, i.e., solvent separated ion pairs (SSIPs), are prevalent in these electrolytes and that the solution dielectric constant, which is increased by the presence of dipolar ion pairs, is critical for controlling these interactions. These findings thus provide a basis for understanding the physical chemistry of multivalent battery electrolytes.

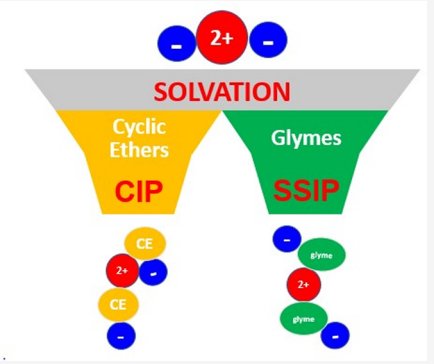

INTRODUCTION

The major role of the electrolyte in a battery system is transferring active ions between the two electrodes (cathode and anode) in accordance with the charge/discharge process. In addition to this primary role, electrolytes often decompose at electrode/electrolyte interfaces to form a solid-electrolyte interphase (SEI) layer, making sustainable battery operation possible in the case of alkali metals (Li^+, etc.). For multivalent secondary batteries, however, such interphases are not sufficiently ionically conductive, making electrolyte stability an important property defining battery performance. It has become increasingly clear that electrolyte stability, as well as additional electrolyte properties, depends greatly on the sub-nanoscale interactions of salt and solvent species constituting the solvation environment. Hence, understanding how this environment can be manipulated through salt and solvent selection has become critical to the progress of advanced battery chemistries. Much of the current research in multivalent batteries is focused on non-aqueous Mg^{2+} chemistries and aqueous Zn^{2+} chemistries. However, there is growing interest in non-aqueous Ca^{2+} and Zn^{2+} chemistries,[1−7] providing an intriguing opportunity to connect scientific understanding across multiple systems. Many of the major Mg^{2+} electrolyte discoveries have utilized ethereal solvents such as tetrahydrofuran (THF) as the solvent of choice due to good reductive stability and favorable coordination of cations, supporting Mg^{2+} complexes capable of depositing Mg with

Received: October 31, 2020
Revised: February 20, 2021
Published: March 11, 2021

high Coulombic efficiency while minimizing passivation.[8−13] Perhaps unsurprisingly, the first electrolyte demonstrating high-efficiency Ca deposition at room temperature also employed THF ($Ca(BH_4)_2$/THF).[1] In addition to its demonstrated importance in the development of multivalent battery electrolytes, THF can be further modified through, for example, methylation at the 2-position yielding 2-methyltetrahydrofuran (2-MeTHF). This modification imbues the electrolyte with new properties, such as improved stability toward reactive metals and some acids.[14,15] 2-MeTHF also demonstrates improved solubility of salts such as $MgBr_2$, MgI_2, and magnesium bis(trifluoromethylsulfonyl)imide ($MgTFSI_2$) as well as other unique properties in organometallic chemistry.[9,16] Linear glyme solvents such as 1,2-dimethoxyethane (G1) or triglyme (G3) represent a different structural class that retains the ether moiety, and such solvents have also been important for developing Mg battery electrolytes.[17−20] Given the growing knowledge of Mg^{2+} electrolytes, investigation into other multivalent electrolytes based on Ca^{2+} or Zn^{2+} provides insight into cation-dependent trends that broaden scientific understanding and aid in developing new multivalent batteries. For example, we have previously compared electrolytes based on $Mg(BH_4)_2$ and $Ca(BH_4)_2$ salts, finding that the differing coordination tendencies of the two cations leads to dramatic differences in electrolyte conductivity and electrochemical behavior.[21] We have also observed that the ethereal solvent/Ca^{2+} cation coordination strength influences electrochemical behavior in electrolytes utilizing more typical weakly coordinating anions.[22] Ponrouch et al. also studied a wide range of Ca^{2+} salts in various aprotic solvents, demonstrating that a wide variety of physo-chemical properties could be achieved.[23] Burrell et al. similarly studied a variety of aprotic Zn^{2+} electrolytes.[4] In this work, our goal is to build on the aforementioned studies by comparing Ca^{2+} and Zn^{2+} solvation properties in ethereal solvents. Understanding how the coordination tendencies of these multivalent cations vary across the cyclic to linear ethereal solvent structure provides insight into the structure−property relationships of these systems, enabling a deeper understanding of rational electrolyte design and informing the broader field of nonaqueous electrolyte physical chemistry. Specifically, we address the question of how the structure of the ether solvent and the size of the divalent cation control anion interaction tendencies. These tendencies are critical for determining the solubility, transport, and even stability properties of multivalent electrolytes. In this work, the interactions of multivalent cations with supporting electrolyte constituents have been examined with PFG-NMR measurements of diffusion. These studies are focused on Zn^{2+} and Ca^{2+} electrolytes consisting of two cyclic ether representatives (THF and 2-MeTHF, Scheme 1) and two glyme representatives (G1 and G3, Scheme 1) using bis(trifluoromethylsulfonyl)imide (TFSI) as a benchmark anion. The TFSI anion was selected due to its importance to a wide variety of battery electrolyte concepts, including Li−O_2, Li−S, and water-in-salt systems for Li-ion or Zn batteries.[24−28] Furthermore, multivalent salts of this anion are commercially available and are readily probed via NMR and vibrational spectroscopy.[29] By combining the PFG-NMR studies with analysis of ion populations through Raman spectroscopy and ionic conductivity measurements, a multifaceted understanding of inter-ionic interactions that bridges across differences in cation size (ionic radius, r_{ion} of Zn^{2+} = 0.74 Å and Ca^{2+} = 0.99 Å),[30] solvent structure, and salt concentration is offered.

Scheme 1. Chemical Structures of (a) Glyme (G1), (b) Triglyme (G3), (c) Tetrahydrofuran (THF), and (d) 2-Methyl-tetrahydrofuran (2-MeTHF)

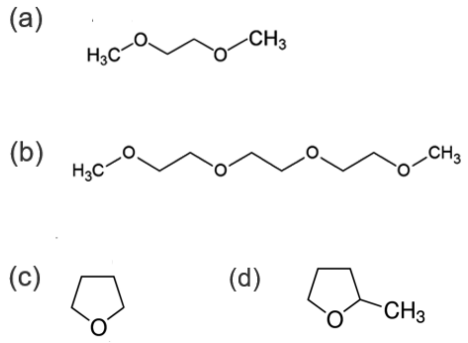

EXPERIMENTAL METHODS

Sample Preparations. $Zn(TFSI)_2$ (99.5%) and $Ca(TFSI)_2$ (99.5%) purchased from Solvionic and dried under vacuum at 160 °C prior to use. Solvents used in this study were purchased from Sigma-Aldrich and dried over activated alumina and molecular sieves yielding a water content of <10 ppm. All reagent handling was performed in a glovebox with $[H_2O]$ < 1 ppm and $[O_2]$ < 0.1 ppm. Various electrolyte formulations were synthesized by weighing out a prescribed mass of salt and adding sufficient solvent to achieve a target solution volume. Two concentrations were targeted in each electrolyte system to establish rudimentary concentration trends: 0.1 and 0.5 M. Most multivalent electrolytes based on ethereal solvents exhibit optimum performance within this concentration range. However, solubility limitations prevented achieving these concentrations in some notable instances. In $Zn(TFSI)_2$/G1 we find that phase separation occurs at intermediate concentrations (between approximately 0.035 and 0.4 M), a surprising phenomenon that also occurs in $Mg(TFSI)_2$/G1 across a similar concentration range,[31] suggesting that cation size plays a role in this behavior. In $Zn(TFSI)_2$/THF, salt solubility is limited to less than 5 mM. In these cases, the concentrations of the insoluble formulations were adjusted systematically by further solvent addition to determine the limiting concentration values. Table 1 contains the final concentrations employed in this study.

PFG-NMR Measurements. All PFG-NMR measurements were performed on a 600 MHz NMR spectrometer (Agilent, USA) with a 5 mm liquid NMR probe. Diffusion coefficients (D) of $TFSI^-$ anions and solvent molecules were determined from ^{19}F and ^1H PFG-NMR, respectively, at 25 °C using the

Table 1. Salt Concentrations Tested within Each Electrolyte System

salt	solvent	concentration (M)	
		low	high
$Zn(TFSI)_2$	G1	0.035	0.5
	G3	0.1	0.5
	THF	0.0008	0.004
	2-MeTHF	0.1	0.5
$Ca(TFSI)_2$	G1	0.1	0.45
	G3	0.1	0.5
	THF	0.1	0.5
	2-MeTHF	0.1	0.5

https://dx.doi.org/10.1021/acs.jpcc.0c09830
J. Phys. Chem. C 2021, 125, 6005−6012

bipolar gradient stimulated echo sequence (Dbppste, vendor supplied sequence, VNMRJ, Agilent). The PFG-echo profiles were recorded as a function of gradient strength with 16 equal steps and fitted with the Stejskal–Tanner equation:[32]

$$S(g) = S(0)\exp[-D(\gamma g\delta)^2(\Delta - \delta/3)] \quad (1)$$

where $S(g)$ and $S(0)$ are the echo heights at the gradient strengths of g and 0, respectively; D is the diffusion coefficient; γ is the gyromagnetic ratio of ^{1}H or ^{19}F; Δ is the diffusion delay, which is the time interval between the two pairs of bipolar pulse gradients; and δ is the gradient length. The time interval Δ and δ were fixed at 30 and 2 ms, respectively, and the maximum gradient strength was accordingly varied to obtain the full decay on the PFG-echo profiles. It was not possible to determine the diffusion coefficients of cations (Zn^{2+} and Ca^{2+}) using PFG-NMR due to fast nuclear relaxation resulting in a null signal after application of the PFG pulse sequence.

Raman Spectroscopy and Ionic Conductivity Measurements. Raman spectroscopy was performed on solutions sealed in glass vials using a Witec Confocal Raman Microscope equipped with a 532 nm laser. Deconvolution of the TFSI breathing mode region (~740 cm^{-1}) was performed using Lorentzian/Gaussian components, similar to published methods.[33,34] Select examples are shown in the Supporting Information. Ionic conductivity measurements were performed using electrochemical impedance spectroscopy in a custom cell containing two parallel Pt electrodes. The cell constant was calibrated using multiple concentrations of KCl in water. Molar equivalent ionic conductivities (Λ_M) were calculated by dividing the measured ionic conductivity value by the solution concentration.

Dielectric Relaxation Spectroscopy Measurements. Solution dielectric constants were measured using dielectric relaxation spectroscopy (DRS). DRS measurements were performed in glass vials using a dielectric probe (Keysight N1501A) and vector network analyzer (Keysight P9375A). The complex permittivity was measured from 0.5 to 26.5 GHz and the experimental data was fit using Debye relaxation processes for solvent and salt components. Extrapolation of the fitted spectra to zero frequency yields the dielectric constant of each solution.[35] Further details are provided in the Supporting Information.

RESULTS AND DISCUSSION

Relative anion and solvent diffusivities depend on both solvent structure and salt concentration and provide insight into the preferential interactions of anion and solvent with multivalent cations. Diffusion coefficients measured by PFG-NMR for all samples are presented in Figure 1a. The results show that the diffusion coefficients tend to be inversely proportional to the viscosity of the solvents (Table 2) as predicted by the Stokes–Einstein relation:

$$D = \frac{k_B T}{6\pi\eta r_s} \quad (2)$$

where k_B is the Boltzmann constant, T is absolute temperature, η is solution viscosity, and r_s is the hydrodynamic radius of the diffusing molecules.[38] In every electrolyte system, the diffusion coefficients of both anion and solvent decrease at the higher concentration value due to an attendant increase in viscosity. While the magnitudes of the diffusion coefficients are closely

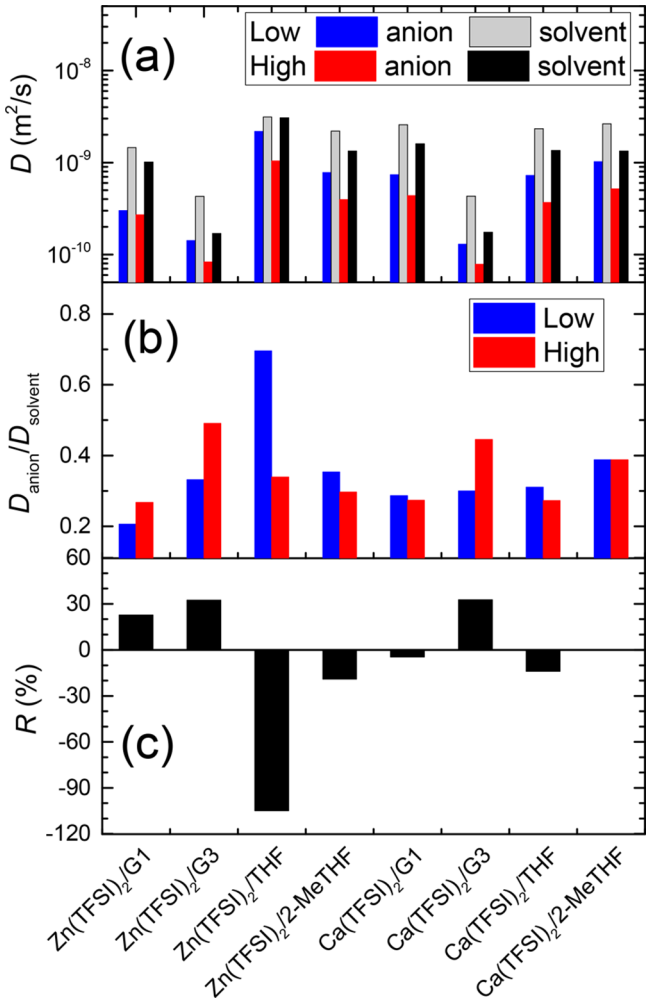

Figure 1. (a) Diffusion coefficients of TFSI anion and solvent molecules (G1, G3, THF, or 2-MeTHF) and (b) diffusion ratios between anion and solvent ($D_{anion}/D_{solvent}$) for different salt concentrations and cation/solvent pairs. (c) Relative change (R) of the diffusion ratio ($D_{anion}/D_{solvent}$) observed after increasing the salt concentration by a factor of ~5. Actual concentrations are provided in Table 1. The actual D values are reported in Table S1.

Table 2. Literature Viscosity and Dielectric Constant (ϵ_r) for G1, G3, THF, and 2-MeTHF Solvents[36]

solvents	viscosity (mPa·s)	ϵ_r
G1	0.46	7.2
G3	1.89	7.5
THF	0.55	7.6
2-MeTHF	0.55[37]	6.97

related to the viscosity of solution, these values also depend upon the interactions of these species with one another. Usually, the measured diffusion coefficient (D) is the weighted average of the diffusion coefficient of free ions/molecules (D_{free}) and the diffusion coefficient of ions/molecules coordinated to the other components of the solution (D_{bound}). In aprotic electrolyte solutions, the interaction between anions and solvent molecules is generally negligible, so the measured diffusion coefficient of anion (D_{anion}) and solvent molecule ($D_{solvent}$) are well-represented by the following relationships:

$$D_{anion} = \alpha D_{free\ anion} + (1 - \alpha)D_{cation-anion} \quad (3)$$

https://dx.doi.org/10.1021/acs.jpcc.0c09830
J. Phys. Chem. C 2021, 125, 6005–6012

and

$$D_{\text{solvent}} = \beta D_{\text{free solvent}} + (1-\beta) D_{\text{cation-solvent}} \quad (4)$$

where α and β are the fractions of free anions and solvent molecules contributing to the measured D_{anion} and D_{solvent}, respectively. On the basis of the Stokes–Einstein relation (eq 2), where D is inversely proportional to the hydrodynamic radius (r_s) of the diffusing molecules, eqs 3 and 4 can be rewritten as follows:

$$\frac{1}{r_{\text{anion}}} = \alpha\left(\frac{1}{r_{\text{s,anion}}}\right) + (1-\alpha)\left(\frac{1}{r_{\text{anion-cation}}}\right) \quad (5)$$

and

$$\frac{1}{r_{\text{solvent}}} = \beta\left(\frac{1}{r_{\text{s,solvent}}}\right) + (1-\beta)\left(\frac{1}{r_{\text{solvent-cation}}}\right) \quad (6)$$

Here $r_{\text{s,anion}}$ and $r_{\text{s,solvent}}$ are the hydrodynamic radii of the free anion and solvent, respectively, and $r_{\text{anion-cation}}$ and $r_{\text{solvent-cation}}$ are the hydrodynamic radii of the complexes containing anions and solvent molecules bound to the cation, respectively. From eqs 5 and 6, the effective hydrodynamic radii of anions (r_{anion}) and solvent molecules (r_{solvent}) will change as the solution fractions of free anion and free solvent change. Since the magnitudes of the measured diffusion coefficients are viscosity dependent, it is useful to compare the ratio of anion to solvent diffusivity, $D_{\text{anion}}/D_{\text{solvent}}$ ($\propto r_{\text{solvent}}/r_{\text{anion}}$), in each solution in order to eliminate the viscosity contribution. This allows one to understand the relative participation of bound anion ($1-\alpha$) and bound solvent ($1-\beta$) within the cation complexes as a function of cation size, solvent structure, and concentration. The diffusion ratios $D_{\text{anion}}/D_{\text{solvent}}$ for these multivalent cation electrolyte solutions are plotted in Figure 1b, and their relative changes after moving from low to high concentration are plotted in Figure 1c. In THF and 2-MeTHF, the $D_{\text{anion}}/D_{\text{solvent}}$ value decreased with an increase in salt concentration for both Ca^{2+} and Zn^{2+}. This means that as the salt concentration increases the effective r_{anion} increases relative to r_{solvent}, reflecting a situation in which the anion:cation interactions are stronger than the solvent/cation interactions. The most dramatic decrease in $D_{\text{anion}}/D_{\text{solvent}}$ among these solutions was observed for $Zn(TFSI)_2$/THF, which was tested at much lower concentrations (where β is ~1) due to poor solubility. This abrupt decrease thus signals an enhancement in TFSI coordination for the higher salt concentration (*vide infra*). For the glyme-based solutions, the $D_{\text{anion}}/D_{\text{solvent}}$ ratio increased with an increase in salt concentration in all cases except $Ca(TFSI)_2$/G1. The increased diffusivity ratio indicates that the solvent–cation interactions are stronger than the anion–cation interactions, i.e., r_{solvent} increases relative to r_{anion} since a greater fraction of total solvent is bound to the cations when the cation concentration is increased. The superior coordination strength of the glyme solvents relative to cyclic ethers is consistent with previous spectroscopic analyses of Mg^{2+} and Ca^{2+} salts.[22,39] The unique behavior of $Ca(TFSI)_2$/G1 among the glyme-based electrolytes indicates that the interaction between G1 and Ca^{2+} is relatively weak, and this is likely related to the larger coordination shell of Ca^{2+} relative to Zn^{2+} yielding different geometric constraints. The larger $D_{\text{anion}}/D_{\text{solvent}}$ values measured for the G3-based solutions compared to that of G1-based solutions for both $Ca(TFSI)_2$ and $Zn(TFSI)_2$ salts implies that G3 interacts more strongly with both cations leading to even greater salt dissociation and significant incorporation of G3 into the cation complexes. A previous investigation indicated that such coordination strength differences are important for determining electrochemical behavior.[22] Overall, the changes in $D_{\text{anion}}/D_{\text{solvent}}$ measured as a function of concentration indicate that anions interact more strongly with multivalent cations in cyclic ethers than in glymes and that the larger size of Ca^{2+} leads to an additional dependence of these interactions on glyme chain length. These results reveal the importance of solvent structure and its determination of specific cation interactions as a driver for the formation of free ions.

The differences in specific anion–cation interactions between Zn^{2+} and Ca^{2+} electrolytes in these ethereal solvents are confirmed through Raman spectroscopy. A direct comparison of $Zn(TFSI)_2$ and $Ca(TFSI)_2$ both as neat salts and in the four solvent systems is shown in Figure 2a,b, focusing on the TFSI breathing mode. Generally, this mode is quite sensitive to different coordination environments and has been studied extensively.[22,33,34,40] Uncoordinated TFSI anions

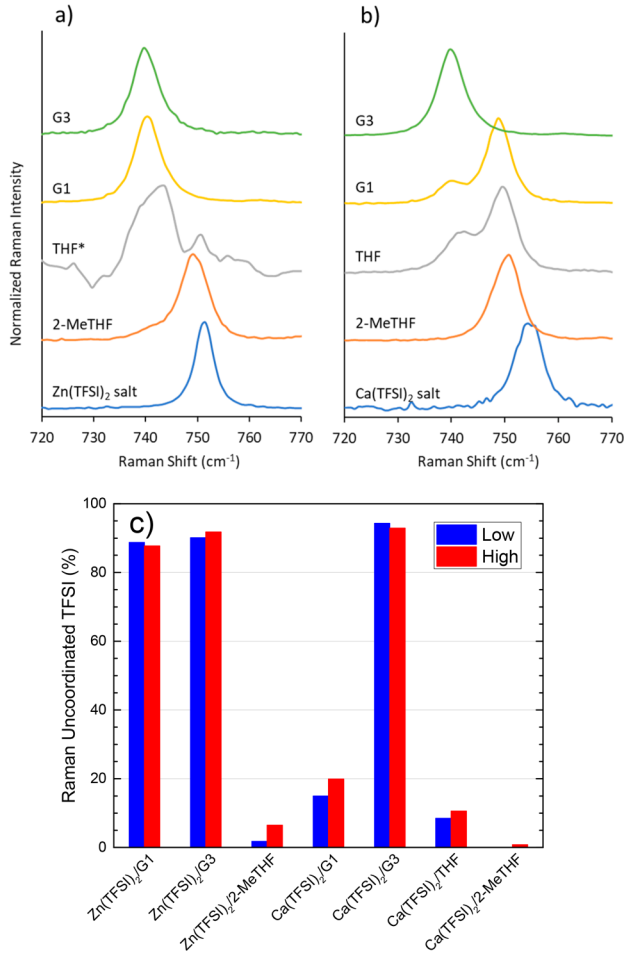

Figure 2. (a, b) Measured Raman spectra for the "high" concentration solutions of (a) $Zn(TFSI)_2$ and (b) $Ca(TFSI)_2$, focusing on the TFSI anion breathing mode. The low signal-to-noise ratio of the $Zn(TFSI)_2$/THF solution is due to the low solubility limit of ~4 mM. (c) Percentage of uncoordinated TFSI measured by Raman spectroscopy within each electrolyte as a function of "low" vs "high" concentration (see Table 1). $Zn(TFSI)_2$ data is excluded due to poor signal-to-noise ratio.

https://dx.doi.org/10.1021/acs.jpcc.0c09830
J. Phys. Chem. C 2021, 125, 6005–6012

yield a symmetric peak at approximately 740 cm^{-1}, while anions interacting directly with a high charge density cation exhibit a blue-shift to frequencies ranging from 742 cm^{-1} to over 750 cm^{-1}, depending on their extent of interaction with the cation. Intimate, multidentate interactions via multiple TFSI oxygens appear to lead to the largest frequency shifts, although explicit structural assignments are generally problematic. In our measurements, the spectra for the neat TFSI salts both yield peak Raman shifts of at least 750 cm^{-1}, signaling intimate TFSI−cation interactions present in the absence of coordinating solvent. When both salts are dissolved in 2-MeTHF these frequencies are red-shifted, but only slightly, and uncoordinated TFSI is only scarcely detectable in the Zn^{2+} case. This indicates that extensive TFSI interaction with both Zn^{2+} and Ca^{2+} persists in 2-MeTHF. In THF, which lacks the steric hindrance of the methyl group, significant changes occur in the Raman peaks that are consistent with increased solvent coordination and decreased anion interaction. Most notably, a peak near 740 cm^{-1} is now observed for both Zn^{2+} and Ca^{2+}, indicating that some dissociation of TFSI from the cation has occurred. Dissociation appears to be greater for Zn^{2+} than for Ca^{2+}, but the low salt concentration of the former makes a nuanced comparison difficult. In G1, however, these differences become more obvious. In this solvent $Zn(TFSI)_2$ is clearly well-dissociated since only the 740 cm^{-1} peak can be observed. In contrast, $Ca(TFSI)_2$ is only slightly dissociated, and its spectra is still dominated by the blue-shifted Raman peak. This demonstrates that the relative anion−cation interactions are stronger in the Ca^{2+} case, which is somewhat surprising given its charge density is lower than that of Zn^{2+}. Recently reported AIMD-metadynamics simulations indicated that G1−Ca^{2+} coordination is somewhat weak and flexible, allowing TFSI to interact more strongly.[22] It appears that G1−Zn^{2+} coordination, however, is much stronger, thus suppressing the TFSI−Zn^{2+} interactions. In G3, both Zn^{2+} and Ca^{2+} possess a single Raman peak, indicating that most of the TFSI is not directly coordinated to Zn^{2+} or Ca^{2+}. This reveals the strong coordination of G3 to dications of either size, consistent on previous work in Ca^{2+} electrolytes.[22]

Raman spectral fitting quantitatively differentiates the coordinating TFSI anion populations in each electrolyte (Figure 2c). Deconvolution of the TFSI breathing mode region of the Raman spectra near 740 cm^{-1} allows estimation of the relative concentration of TFSI that is not directly coordinated to a cation (see the Supporting Information for examples).[33,40] Applying this analysis to these solutions reveals that uncoordinated TFSI populations of over 50% are only achieved in three electrolytes: $Zn(TFSI)_2$/G1, $Zn(TFSI)_2$/G3, and $Ca(TFSI)_2$/G3. In all other solutions over 50% of the TFSI is bound to the cation, indicating these solutions contain primarily contact ion pairs or aggregates rather than free ions. The delineation of these two groups of electrolytes corresponds directly to the observed grouping of positive and negative diffusivity ratio changes observed by PFG-NMR (Figure 1c): Electrolytes with a low TFSI coordination percentage exhibit a positive $D_{anion}/D_{solvent}$ correlation with concentration while electrolytes with a high TFSI coordination percentage exhibit a negative correlation. These relationships demonstrate the impact of inter-ionic interactions on the relative anion and solvent diffusivity. The fact that $D_{anion}/D_{solvent}$ decreases with concentration in the latter group despite a small increase in measured percentage of uncoordinated TFSI ions at higher concentration in these solutions indicates that the motion of the "liberated" TFSI anions remains largely correlated to the metal cation. Therefore, the diffusing cluster size increases as TFSI is displaced from the first shell to the second shell forming a solvent-separated ion pair (SSIP), resulting in a lower diffusivity value. The Raman results show that the percentage of uncoordinated TFSI is more dependent on solvent structure than on concentration, i.e., the largest changes occur between electrolytes containing different solvents rather than between the lower and higher salt concentrations within the same solvent. This relationship highlights the dominant role of solvent structure in determining the general extent of direct anion−cation interactions within this concentration range, implying the importance of specific solvent−cation interactions for determining electrolyte speciation. For example, the glyme solvents likely provide more efficient oxygen−cation coordination due to their ability to form multidentate chelate structures unlike the cyclic ethers, which contain only a single oxygen atom attached to a bulkier ring structure. The importance of these specific interactions is also implied by the lack of correlation between the uncoordinated TFSI percentage differences and the relatively consistent solvent dielectric constants (Table 2). The only glyme-based electrolyte that does not show preferential solvent−cation interactions based on the Raman and diffusivity analyses is $Ca(TFSI)_2$/G1. These findings suggest that the larger size of Ca^{2+} (r_{ion} = 0.99 Å) compared to that of Zn^{2+} (r_{ion} = 0.74 Å) imposes a less favorable geometry for complete multidentate chelation by several shorter glyme molecules. Taken together, these results demonstrate that specific solvent−cation interactions are critical for determining the extent of anion−cation interactions in multivalent electrolytes and the resulting speciation.

By controlling both ion populations and dynamics, a solvent's structure and therefore its specific interaction with multivalent cations strongly influences the ionic conductivity of ethereal multivalent electrolytes. However, by comparing the concentration dependence of molar ionic conductivity (Λ_M) within each solution, we find that nonspecific, long-range interactions are also important for regulating the de-correlation of ion motion, i.e., ionicity. The impact of solvent and concentration on Λ_M is shown in Figure 3. Since ionic

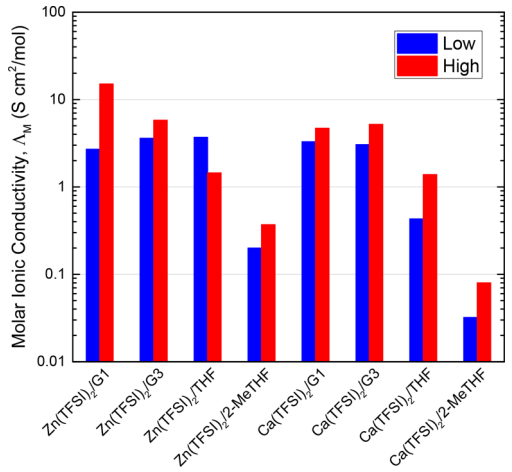

Figure 3. Concentration-normalized ionic conductivities measured for the indicated electrolytes as a function of "low" vs "high" concentration (see Table 1).

https://dx.doi.org/10.1021/acs.jpcc.0c09830
J. Phys. Chem. C 2021, 125, 6005−6012

conductivity represents the combined influence of ion populations (as measured by Raman) and ion mobility (as measured by PFG-NMR), the trend in which cyclic ether solvents yield lower conductivities than glyme solvents is not surprising. However, the concentration dependence is surprising: All but one of the electrolyte systems show a significant increase in Λ_M when concentration is increased, indicating an increase in effective ionicity. Conventional intuition would predict ionicity to decrease with increasing salt concentration due to a lower average inter-ionic spacing and a decrease in relative solvent concentration. However, low permittivity solvents often exhibit a non-intuitive Λ_M increase with concentration at moderate to high salt concentrations.[41−43] While originally such behavior was typically attributed to the formation of triple ions,[43] newer insight suggests that an increase in solution dielectric constant due to the presence of dipolar ion pairs induces more effective screening of Coulombic interactions between the ionic species and thus an increased Λ_M.[35,41,44] In our measurements, the increase in Λ_M at high concentrations is not generally commensurate with the small changes in uncoordinated TFSI populations measured by Raman. This suggests that the increased Λ_M is primarily driven by decreased correlation of separated ion motion, i.e., dissociation of SSIPs, rather than by enhanced dissociation of bound CIPs. To determine whether this may be related to an increase in the dielectric constant of these solutions, we performed DRS as a function of salt concentration in three electrolytes: $Ca(TFSI)_2$/G1, $Ca(TFSI)_2$/G3, and $Zn(TFSI)_2$/G1. DRS reveals that the dielectric constants of all three electrolyte solutions increase significantly above that of the neat solvent, reaching values of 14 or greater (Figure 4a). This confirms that dipolar ion pairs, observed in the low-frequency region of the microwave DRS spectra (Figure 4b−d), increase the dielectric constant. These ion pairs likely include both CIPs and SSIPs. Furthermore, the slope of the ε_r versus concentration trend generally decreases with increase salt concentration, which indicates that the fraction of these dipolar ion pairs decreases at high salt concentrations. These observations suggest that dipolar ion pairs aid in the dissociation of tightly correlated ions, although additional nuances exist depending on the speciation present in each system. For example, a system with strong anion−cation interactions, $Ca(TFSI)_2$/G1, exhibits the greatest increase in dielectric constant since it has the largest population of CIPs, whereas a system with far fewer CIPs, $Ca(TFSI)_2$/G3, exhibits a smaller increase in dielectric constant. Nevertheless, this change is apparently sufficient to decorrelate the SSIPs present in that system.

These findings demonstrate that second-shell interactions, e.g., SSIP species to which Raman is insensitive, are prevalent even in weakly coordinating multivalent electrolytes and are thus important for determining the ionic conductivity in these systems. Hence, strong specific solvent−cation interactions do not guarantee that cation and anion dynamics are uncorrelated. The lone electrolyte tested that exhibits a decrease in Λ_M with increasing concentration is $Zn(TFSI)_2$/THF. We attribute the uniqueness of this electrolyte's behavior to its much lower measured concentration range (on the order of 1 mM). At such concentrations, these solutions approach a more idealized dilute regime in which the average solution inter-ionic distance is similar to the Bjerrum length of THF (~7 nm).[45] In this case the intrinsic permittivity of the solvent alone is effective at de-correlating ion motion, and ion correlations therefore

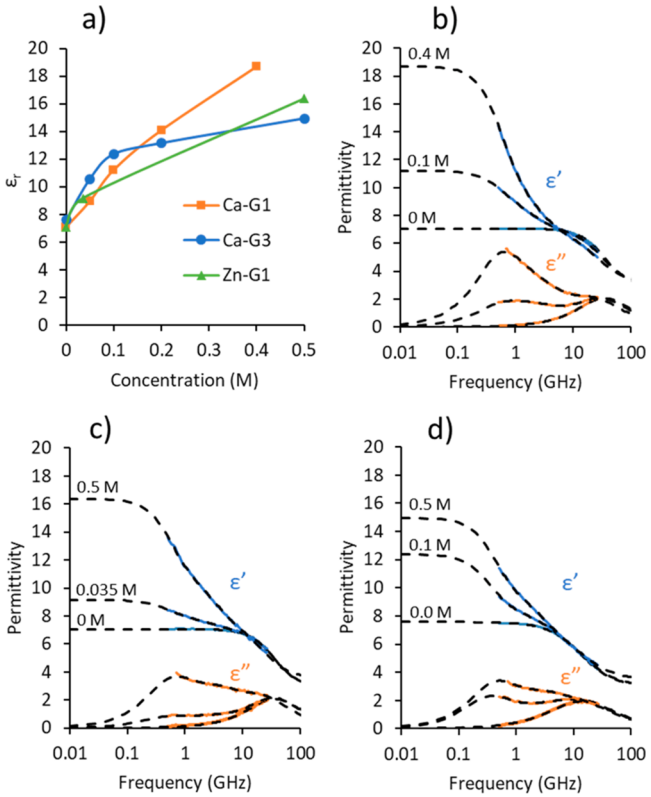

Figure 4. (a) Dielectric constants plotted as a function of salt concentration in $Ca(TFSI)_2$/G1, $Ca(TFSI)_2$/G3 and $Zn(TFSI)_2$/G1. (b−d) Measured (solid lines) and fitted (dashed lines) DRS spectra showing the frequency-dependent real (ε') and imaginary (ε'') permittivities of (b) $Ca(TFSI)_2$/G1, (c) $Zn(TFSI)_2$/G1, and (d) $Ca(TFSI)_2$/G3.

increase with increasing salt concentration. Consistent with this, the $D_{anion}/D_{solvent}$ decrease as measured by PFG-NMR in this electrolyte is much greater than that of any other electrolyte (Figure 1). In summary, the measured Λ_M trends confirm the relative differences in specific anion−cation interaction strength between cyclic ether solutions and glyme solutions while also revealing the importance of nonspecific interactions for determining the extent of correlated ion motion, particular in the strongly interacting glyme solvents.

CONCLUSIONS

In conclusion, we have addressed the question of how solvent structure and cation size influence the cation−anion interaction tendencies of ethereal multivalent electrolytes and their resulting correlated dynamics. These investigations were conducted using PFG-NMR, Raman spectroscopy, and ionic conductivity measurements across two sets of cation sizes, salt concentrations, and ethereal solvent structures. The results show that specific solvent−cation interactions are stronger for glymes than those for cyclic ethers leading to weaker anion−cation interactions in the former. Ca^{2+} generally interacts more strongly with anions than does Zn^{2+} despite having a lower charge density, and this is especially obvious in G1. The unexpected increase in Λ_M measured for all electrolytes when concentration is increased from ~0.1 to ~0.5 M implies that second-shell ion correlations are prevalent in this class of solvents, regardless of variation in specific interactions, due to their low dielectric constants. As a result, perturbations to the

https://dx.doi.org/10.1021/acs.jpcc.0c09830
J. Phys. Chem. C 2021, 125, 6005−6012

overall solution permittivity by dipolar ion pairs appears to be a general mechanism for de-correlating ion motion in relatively well-dissociated multivalent electrolytes. Using dielectric relaxation spectroscopy in select cases, we have confirmed that dipolar ion pairs can indeed play such a role. Further multimodal studies are needed to elucidate correlation between ion-pair motion and permittivity of multivalent electrolyte solutions. These findings add to the broader understanding of non-aqueous electrolyte physical chemistry while also providing a basis for developing design rules for multivalent electrolytes.

■ ASSOCIATED CONTENT

Supporting Information

The Supporting Information is available free of charge at https://pubs.acs.org/doi/10.1021/acs.jpcc.0c09830.

Diffusion coefficients of the tested series of samples, select examples of Raman spectral deconvolution used to quantify uncoordinated TFSI populations, and additional DRS experimental details, parameters, and deconvoluted spectra (PDF)

■ AUTHOR INFORMATION

Corresponding Authors

Vijayakumar Murugesan − *Pacific Northwest National Laboratory, Richland, Washington 99352, United States; Joint Center for Energy Storage Research (JCESR), Lemont, Illinois 60439, United States;* orcid.org/0000-0001-6149-1702; Email: vijay@pnnl.gov

Karl T. Mueller − *Pacific Northwest National Laboratory, Richland, Washington 99352, United States; Joint Center for Energy Storage Research (JCESR), Lemont, Illinois 60439, United States;* orcid.org/0000-0001-9609-9516; Email: karl.mueller@pnnl.gov

Authors

Kee Sung Han − *Pacific Northwest National Laboratory, Richland, Washington 99352, United States; Joint Center for Energy Storage Research (JCESR), Lemont, Illinois 60439, United States;* orcid.org/0000-0002-3535-1818

Nathan T. Hahn − *Joint Center for Energy Storage Research (JCESR), Lemont, Illinois 60439, United States; Sandia National Laboratories, Albuquerque, New Mexico 87185, United States;* orcid.org/0000-0001-6187-4068

Kevin R. Zavadil − *Joint Center for Energy Storage Research (JCESR), Lemont, Illinois 60439, United States; Sandia National Laboratories, Albuquerque, New Mexico 87185, United States;* orcid.org/0000-0002-3791-424X

Nicholas R. Jaegers − *Pacific Northwest National Laboratory, Richland, Washington 99352, United States;* orcid.org/0000-0002-9930-7672

Ying Chen − *Pacific Northwest National Laboratory, Richland, Washington 99352, United States; Joint Center for Energy Storage Research (JCESR), Lemont, Illinois 60439, United States;* orcid.org/0000-0001-7417-0991

Jian Zhi Hu − *Pacific Northwest National Laboratory, Richland, Washington 99352, United States; Joint Center for Energy Storage Research (JCESR), Lemont, Illinois 60439, United States;* orcid.org/0000-0001-8879-747X

Complete contact information is available at: https://pubs.acs.org/10.1021/acs.jpcc.0c09830

Author Contributions

#K.S.H. and N.T.H. contributed equally to this work.

Notes

The authors declare no competing financial interest.

■ ACKNOWLEDGMENTS

This research was led intellectually by researchers within the Joint Center for Energy Storage Research (JCESR), an Energy Innovation Hub funded by the U.S. Department of Energy (DOE), Office of Science, Basic Energy Sciences (BES). The NMR measurements were performed at the Environmental Molecular Sciences Laboratory (EMSL), a national scientific user facility sponsored by the DOE's Office of Biological and Environmental Research and located at Pacific Northwest National Laboratory (PNNL). PNNL is a multiprogram laboratory operated for the DOE by Battelle under Contract DE-AC05-76RL01830. Sandia National Laboratories is a multimission laboratory managed and operated by National Technology & Engineering Solutions of Sandia, LLC, a wholly owned subsidiary of Honeywell International, Inc., for the DOE's National Nuclear Security Administration under contract DE-NA0003525. This paper describes objective technical results and analysis. Any subjective views or opinions that might be expressed in the paper do not necessarily represent the views of the U.S. Department of Energy or the United States Government.

■ REFERENCES

(1) Wang, D.; Gao, X.; Chen, Y.; Jin, L.; Kuss, C.; Bruce, P. G. Plating and Stripping Calcium in an Organic Electrolyte. *Nat. Mater.* **2018**, *17*, 16−20.

(2) Ponrouch, A.; Frontera, C.; Bardé, F.; Palacín, M. R. Towards a Calcium-Based Rechargeable Battery. *Nat. Mater.* **2016**, *15*, 169−172.

(3) Ta, K.; Zhang, R.; Shin, M.; Rooney, R. T.; Neumann, E. K.; Gewirth, A. A. Understanding Ca Electrodeposition and Speciation Processes in Nonaqueous Electrolytes for Next-Generation Ca-Ion Batteries. *ACS Appl. Mater. Interfaces* **2019**, *11*, 21536−21542.

(4) Han, S.-D.; Rajput, N. N.; Qu, X.; Pan, B.; He, M.; Ferrandon, M. S.; Liao, C.; Persson, K. A.; Burrell, A. K. Origin of Electrochemical, Structural, and Transport Properties in Nonaqueous Zinc Electrolytes. *ACS Appl. Mater. Interfaces* **2016**, *8*, 3021−3031.

(5) Jie, Y.; Tan, Y.; Li, L.; Han, Y.; Xu, S.; Zhao, Z.; Cao, R.; Ren, X.; Huang, F.; Lei, Z.; et al. Electrolyte Solvation Manipulation Enables Unprecedented Room-Temperature Calcium-Metal Batteries. *Angew. Chem., Int. Ed.* **2020**, *59*, 12689−12693.

(6) Lapidus, S. H.; Rajput, N. N.; Qu, X.; Chapman, K. W.; Persson, K. A.; Chupas, P. J. Solvation Structure and Energetics of Electrolytes for Multivalent Energy Storage. *Phys. Chem. Chem. Phys.* **2014**, *16*, 21941−21945.

(7) Zhang, R.; Pan, C.; Nuzzo, R. G.; Gewirth, A. A. CoS_2 as a Sulfur Redox-Active Cathode Material for High-Capacity Nonaqueous Zn Batteries. *J. Phys. Chem. C* **2019**, *123*, 8740−8745.

(8) Aurbach, D.; Lu, Z.; Schechter, A.; Gofer, Y.; Gizbar, H.; Turgeman, R.; Cohen, Y.; Moshkovich, M.; Levi, E. Prototype Systems for Rechargeable Magnesium Batteries. *Nature* **2000**, *407*, 724−727.

(9) Kim, H. S.; Arthur, T. S.; Allred, G. D.; Zajicek, J.; Newman, J. G.; Rodnyansky, A. E.; Oliver, A. G.; Boggess, W. C.; Muldoon, J. Structure and Compatibility of a Magnesium Electrolyte with a Sulphur Cathode. *Nat. Commun.* **2011**, *2*, 427.

(10) Doe, R. E.; Han, R.; Hwang, J.; Gmitter, A. J.; Shterenberg, I.; Yoo, H. D.; Pour, N.; Aurbach, D. Novel, Electrolyte Solutions Comprising Fully Inorganic Salts with High Anodic Stability for Rechargeable Magnesium Batteries. *Chem. Commun.* **2014**, *50*, 243−245.

(11) Kim, I.-T.; Yamabuki, K.; Sumimoto, M.; Tsutsumi, H.; Morita, M.; Yoshimoto, N. Characteristics of Tetrahydrofuran-Based Electrolytes with Magnesium Alkoxide Additives for Rechargeable Magnesium Batteries. *J. Power Sources* **2016**, *323*, 51−56.
(12) Liu, T.; Shao, Y.; Li, G.; Gu, M.; Hu, J.; Xu, S.; Nie, Z.; Chen, X.; Wang, C.; Liu, J. A Facile Approach Using $MgCl_2$ to Formulate High Performance Mg^{2+} Electrolytes for Rechargeable Mg Batteries. *J. Mater. Chem. A* **2014**, *2*, 3430−3438.
(13) Liao, C.; Guo, B.; Jiang, D.-e.; Custelcean, R.; Mahurin, S. M.; Sun, X.-G.; Dai, S. Highly Soluble Alkoxide Magnesium Salts for Rechargeable Magnesium Batteries. *J. Mater. Chem. A* **2014**, *2*, 581−584.
(14) Goldman, J. L.; Mank, R. M.; Young, J. H.; Koch, V. R. Structure-Reactivity Relationships of Methylated Tetrahydrofurans with Lithium. *J. Electrochem. Soc.* **1980**, *127*, 1461.
(15) Aycock, D. F. Solvent Applications of 2-Methyltetrahydrofuran in Organometallic and Biphasic Reactions. *Org. Process Res. Dev.* **2007**, *11*, 156−159.
(16) Hattori, M.; Yamamoto, K.; Matsui, M.; Nakanishi, K.; Mandai, T.; Choudhary, A.; Tateyama, Y.; Sodeyama, K.; Uchiyama, T.; Orikasa, Y.; et al. Role of Coordination Structure of Magnesium Ions on Charge and Discharge Behavior of Magnesium Alloy Electrode. *J. Phys. Chem. C* **2018**, *122*, 25204−25210.
(17) Shterenberg, I.; Salama, M.; Yoo, H. D.; Gofer, Y.; Park, J.-B.; Sun, Y.-K.; Aurbach, D. Evaluation of $(CF_3SO_2)_2N^-$(TFSI) Based Electrolyte Solutions for Mg Batteries. *J. Electrochem. Soc.* **2015**, *162*, A7118−A7128.
(18) Tutusaus, O.; Mohtadi, R.; Arthur, T. S.; Mizuno, F.; Nelson, E. G.; Sevryugina, Y. V. An Efficient Halogen-Free Electrolyte for Use in Rechargeable Magnesium Batteries. *Angew. Chem., Int. Ed.* **2015**, *54*, 7900−7904.
(19) Lau, K.-C.; Seguin, T. J.; Carino, E. V.; Hahn, N. T.; Connell, J. G.; Ingram, B. J.; Persson, K. A.; Zavadil, K. R.; Liao, C. Widening Electrochemical Window of Mg Salt by Weakly Coordinating Perfluoroalkoxyaluminate Anion for Mg Battery Electrolyte. *J. Electrochem. Soc.* **2019**, *166*, A1510−A1519.
(20) Hahn, N. T.; Seguin, T. J.; Lau, K.-C.; Liao, C.; Ingram, B. J.; Persson, K. A.; Zavadil, K. R. Enhanced Stability of the Carba-Closo-Dodecaborate Anion for High-Voltage Battery Electrolytes through Rational Design. *J. Am. Chem. Soc.* **2018**, *140*, 11076−11084.
(21) Hahn, N. T.; Self, J.; Seguin, T. J.; Driscoll, D. M.; Rodriguez, M. A.; Balasubramanian, M.; Persson, K. A.; Zavadil, K. R. The Critical Role of Configurational Flexibility in Facilitating Reversible Reactive Metal Deposition from Borohydride Solutions. *J. Mater. Chem. A* **2020**, *8*, 7235−7244.
(22) Hahn, N. T.; Driscoll, D. M.; Yu, Z.; Sterbinsky, G. E.; Cheng, L.; Balasubramanian, M.; Zavadil, K. R. Influence of Ether Solvent and Anion Coordination on Electrochemical Behavior in Calcium Battery Electrolytes. *ACS Applied Energy Materials* **2020**, *3*, 8437−8447.
(23) Forero-Saboya, J. D.; Marchante, E.; Araujo, R. B.; Monti, D.; Johansson, P.; Ponrouch, A. Cation Solvation and Physicochemical Properties of Ca Battery Electrolytes. *J. Phys. Chem. C* **2019**, *123*, 29524−29532.
(24) Kwak, W.-J.; Rosy; Sharon, D.; Xia, C.; Kim, H.; Johnson, L. R.; Bruce, P. G.; Nazar, L. F.; Sun, Y.-K.; Frimer, A. A. Lithium−Oxygen Batteries and Related Systems: Potential, Status, and Future. *Chem. Rev.* **2020**, *120*, 6626.
(25) Manthiram, A.; Fu, Y.; Chung, S.-H.; Zu, C.; Su, Y.-S. Rechargeable Lithium−Sulfur Batteries. *Chem. Rev.* **2014**, *114*, 11751−11787.
(26) Suo, L.; Hu, Y.-S.; Li, H.; Armand, M.; Chen, L. A New Class of Solvent-in-Salt Electrolyte for High-Energy Rechargeable Metallic Lithium Batteries. *Nat. Commun.* **2013**, *4*, 1481.
(27) Suo, L.; Borodin, O.; Gao, T.; Olguin, M.; Ho, J.; Fan, X.; Luo, C.; Wang, C.; Xu, K. "Water-in-Salt" Electrolyte Enables High-Voltage Aqueous Lithium-Ion Chemistries. *Science* **2015**, *350*, 938−943.
(28) Wang, F.; Borodin, O.; Gao, T.; Fan, X.; Sun, W.; Han, F.; Faraone, A.; Dura, J. A.; Xu, K.; Wang, C. Highly Reversible Zinc Metal Anode for Aqueous Batteries. *Nat. Mater.* **2018**, *17*, 543−549.
(29) Hu, J. Z.; Jaegers, N. R.; Hu, M. Y.; Mueller, K. T. In Situ and Ex Situ NMR for Battery Research. *J. Phys.: Condens. Matter* **2018**, *30*, 463001.
(30) Barbalace, K. Periodic Table of Elements - Sorted by Ionic Radius. https://environmentalchemistry.com/yogi/periodic/ionicradius.html (accessed May 21, 2020).
(31) Salama, M.; Shterenberg, I.; Gizbar, H.; Eliaz, N. N.; Kosa, M.; Keinan-Adamsky, K.; Afri, M.; Shimon, L. J. W.; Gottlieb, H. E.; Major, D. T.; et al. Unique Behavior of Dimethoxyethane (DME)/$Mg(N(SO_2CF_3)_2)_2$ Solutions. *J. Phys. Chem. C* **2016**, *120*, 19586−19594.
(32) Stejskal, E. O.; Tanner, J. E. Spin Diffusion Measurements: Spin Echoes in the Presence of a Time-Dependent Field Gradient. *J. Chem. Phys.* **1965**, *42*, 288−292.
(33) Giffin, G. A.; Moretti, A.; Jeong, S.; Passerini, S. Complex Nature of Ionic Coordination in Magnesium Ionic Liquid-Based Electrolytes: Solvates with Mobile Mg^{2+} Cations. *J. Phys. Chem. C* **2014**, *118*, 9966−9973.
(34) Watkins, T.; Buttry, D. A. Determination of Mg^{2+} Speciation in a TFSI−-Based Ionic Liquid with and without Chelating Ethers Using Raman Spectroscopy. *J. Phys. Chem. B* **2015**, *119*, 7003−7014.
(35) Self, J.; Hahn, N. T.; Fong, K. D.; McClary, S. A.; Zavadil, K. R.; Persson, K. A. Ion Pairing and Redissociaton in Low-Permittivity Electrolytes for Multivalent Battery Applications. *J. Phys. Chem. Lett.* **2020**, *11*, 2046−2052.
(36) Scheers, J.; Fantini, S.; Johansson, P. A Review of Electrolytes for Lithium−Sulphur Batteries. *J. Power Sources* **2014**, *255*, 204−218.
(37) Engler, B. P.; Harrah, L. A. Viscosity and Density of 2-Methyltetrahydrofuran as a Function of Temperature. https://inis.iaea.org/search/search.aspx?orig_q=RN:10460457 (accessed March 19, 2020).
(38) Pregosin, P. S.; Kumar, P. G. A.; Fernández, I. Pulsed Gradient Spin−Echo (PGSE) Diffusion and ^1H, ^{19}F Heteronuclear Overhauser Spectroscopy (HOESY) NMR Methods in Inorganic and Organometallic Chemistry: Something Old and Something New. *Chem. Rev.* **2005**, *105*, 2977−2998.
(39) Tuerxun, F.; Yamamoto, K.; Hattori, M.; Mandai, T.; Nakanishi, K.; Choudhary, A.; Tateyama, Y.; Sodeyama, K.; Nakao, A.; Uchiyama, T.; et al. Determining Factor on the Polarization Behavior of Magnesium Deposition for Magnesium Battery Anode. *ACS Appl. Mater. Interfaces* **2020**, *12*, 25775−25785.
(40) Seo, D. M.; Boyle, P. D.; Sommer, R. D.; Daubert, J. S.; Borodin, O.; Henderson, W. A. Solvate Structures and Spectroscopic Characterization of LiTFSI Electrolytes. *J. Phys. Chem. B* **2014**, *118*, 13601−13608.
(41) Cavell, E. A. S.; Knight, P. C. Effect of Concentration Changes on Permittivity of Electrolyte Solutions. *Z. Phys. Chem.* **1968**, *57*, 331.
(42) Delsignore, M.; Farber, H.; Petrucci, S. Ionic Conductivity and Microwave Dielectric Relaxation of Lithium Hexafluoroarsenate ($LiAsF_6$) and Lithium Perchlorate ($LiClO_4$) in Dimethyl Carbonate. *J. Phys. Chem.* **1985**, *89*, 4968−4973.
(43) Fuoss, R. M.; Kraus, C. A. Properties of Electrolytic Solutions. IV. The Conductance Minimum and the Formation of Triple Ions Due to the Action of Coulomb Forces[1]. *J. Am. Chem. Soc.* **1933**, *55*, 2387−2399.
(44) Petrucci, S.; Masiker, M. C.; Eyring, E. M. The Possible Presence of Triple Ions in Electrolyte Solutions of Low Dielectric Permittivity. *J. Solution Chem.* **2008**, *37*, 1031−1035.
(45) Moritz, R.; Zardalidis, G.; Butt, H.-J.; Wagner, M.; Müllen, K.; Floudas, G. Ion Size Approaching the Bjerrum Length in Solvents of Low Polarity by Dendritic Encapsulation. *Macromolecules* **2014**, *47*, 191−196.

https://dx.doi.org/10.1021/acs.jpcc.0c09830
J. Phys. Chem. C 2021, 125, 6005−6012